Upcycled High-Strength Aluminum Alloys from Scrap through Solid-Phase Alloying

Xiao Li

xiao.li@pnnl.gov

Pacific Northwest National Lab https://orcid.org/0000-0003-2096-298X

Tianhao Wang

Pacific Northwest National Laboratory

Zehao Li

Pacific Northwest National Laboratory

Tingkun Liu

Pacific Northwest National Laboratory

Xiang Wang

Pacific Northwest National Laboratory https://orcid.org/0000-0002-9629-3084

Arun Devaraj

Pacific Northwest National Laboratory https://orcid.org/0000-0003-1314-6212

Cindy Powell

Pacific Northwest National Laboratory

Jorge F. dos Santos

Pacific Northwest National Laboratory

Letter

Keywords:

Posted Date: March 25th, 2024

DOI: https://doi.org/10.21203/rs.3.rs-4011560/v1

Additional Declarations: There is **NO** Competing Interest.

Abstract

Although recycling secondary aluminum can lead to energy consumption reduction compared to primary aluminum manufacturing, products produced by traditional melt-based recycling processes are inherently limited in terms of alloy composition and microstructure, and thus final properties. To overcome the constraints associated with melting, we have developed a novel solid-phase recycling and simultaneous alloying method. This innovative process enables the alloying of 6063 aluminum scrap with copper, zinc, and magnesium, to form a nanocluster-strengthened high-performance aluminum alloy with a composition and properties akin to 7075 aluminum alloy. The unique nanostructure with high density of Guinier-Preston zones and uniformly precipitated nanoscale η'/$Mg(CuZn)_2$ strengthening phases, enhances both yield and ultimate tensile strength by > 200%. By delivering high-performance products from scrap that are not just recycled but *upcycled*, this scalable manufacturing approach offers a new paradigm of metals reuse, with the option for on-demand upcycling of a variety of metallic materials from scrap sources.

Main

Aluminum (Al) stands as the most extensively utilized non-ferrous metal globally [1, 2], and the Al industry contributes 3% of all greenhouse gas emissions [3]. This is because the Hall–Héroult process used to produce primary Al from ore emits a significant amount of CO_2 [4]. Using 100% scrap aluminum feedstocks could theoretically reduce energy and carbon emissions by up to 95% compared to primary aluminum production [5, 6]. Nevertheless, this level of reduced environmental impact has not been achieved because scrap inevitably contains undesirable impurities, requiring the addition of primary Al in a process known as “purifying and diluting” [3, 7–10]. Also, the traditional production of secondary Al through recycling involves a number of energy-intensive steps (Fig. 1a). The reliance on primary Al additions, combined with the requirement for high-temperature melting and other processing steps, results in a recycled product that still has a relatively high energy and carbon intensity [3]. In this letter, we report friction extrusion as a solid-phase alloying method to both recycle and upcycle Al scrap to directly produce high-performance Al wrought extrudate in a single step, with a much lower carbon footprint (Fig. 1b). For upcycling, 6063 Al scrap and alloying sources—copper (Cu) powder, zinc (Zn) powder, and ZK60 magnesium (Mg) ribbon—are first physically blended and then subjected to friction extrusion, removing the requirement for bulk melting to incorporate the alloying elements into the Al matrix. The thermo-mechanical nature of the friction extrusion process results in the production of a fine-grained aluminum microstructure with a high-density of strengthening nanoclusters in the extruded product. Because this solid-phase process allows aluminum scrap to be upcycled into high-performance aluminum products without the need for either the addition of primary aluminum or melting, it has the potential to significantly reduce CO_2 emissions [11, 12].

As previously described, the precursor materials used in this work (Fig. 2a) include 6063 Al scrap, with alloying additions of Cu, Zn, and ZK60 Mg. The products of the upcycling process are benchmarked against a recycled 6063 alloy manufactured using the same friction extrusion approach. For the recycled

alloy, cold compacted 6063 scrap was friction extruded to produce a void free, 5 mm diameter rod (Fig. 2b). For the upcycled product, the mixture of 6063 scrap and alloying additions were friction extruded under similar process conditions to produce a void-free rod (Fig. 2c) with a composition close to that of a standard 7075 Al alloy. The recycled rod has an average grain size of 43.1 μm, as shown in the electron backscatter diffraction-inverse pole figure (EBSD-IPF) map in Fig. 2d. The upcycled rod, on the other hand, shows pronounced grain refinement, with an average grain size of 7.7 μm (Fig. 2e). A comparison of the tensile stress-strain curves for the recycled 6063 Al alloy, the upcycled 6063 Al alloy, and a conventional wrought 6063 Al alloy (Fig. 2f), highlights the pronounced increase in yield strength and ultimate tensile strength for the upcycled material. Specifically, upcycling results in a > 200% increase in both the yield strength (from 87 MPa to 263 MPa) and the ultimate tensile strength (from 147 MPa to 443 MPa), when compared to the recycled alloy.

Examining the microstructural evolution during the upcycling process provides insight into the origins of the differences in mechanical properties between recycled and upcycled materials. Optical microscopy of the longitudinal cross-section of the extruded rod and remnant disc (scrap/powders mixture) from the upcycling process (Fig. 3a**)** reveals four distinct processing zones: an unprocessed region consisting of the compacted scrap/alloying additions (Zone A); a transition region (Zone B); a processed region (Zone C); and the extruded rod (Zone D). Process temperatures increase exponentially from Zone A to Zone C, where the highest processing temperature is reached, The colling process begins Zone D. In the present study no forced cooling was applied. Higher magnification scanning electron microscopy (SEM) images, combined with energy dispersive spectroscopy (EDS) maps, from Zones A–D are also included in Fig. 3b. These images show that in Zone A, the 6063 Al scrap is surrounded by Zn powders, ZK60 Mg alloy ribbons, and Cu powders, which are tightly compacted. In Zone B, the alloying additions undergo severe shear deformation and are highly strained, elongated, and fractured. In Zone C, further refining promotes dispersion and diffusion of the alloying additions into the Al matrix, prior to extrusion. In Zone D the extruded product has similar microstructural features to those observed in Zone C. It is clear from these images that the additional alloying elements Zn, Mg, and Cu become progressively more homogeneously distributed in the microstructure as the material is processed from Zone A to B, to C, and finally to D. In other words, these alloying elements are refined and mixed into the Al matrix during the friction extrusion process that took less than a minute to complete, while the Al scrap was simultaneously consolidated into the extrudate [13, 14]. These observations are supported by a hardness map (inset in Fig. 3a**)**, which shows the variation in hardness that results from the above described changes in microstructure. This type of microstructure evolution during friction extrusion has been reported in our previous work on the 7075 Al alloy system [15], and can be attributed to gradients in strain and temperature fields as the material is processed [16, 17].

To confirm homogneity of the microstructure and chemistry of the upcycled and recycled rods, additional microscopy was conducted on both transvere and longitudinal cross-sections, with illustrative results provided in **Fig. S1** (Supplementary Material Section 1). Hardness testing on the cross-sections of both recycled and upcycled rods reveals an average hardness of 43 HV for the recycled rod versus an average hardness 116 HV for the upcycled rod (**Fig. S2**, Supplementary Materials Section 2).

Further microstructural characterization of the recycled and upcycled specimens pinpoints the reason for the substantial strengthening achieved as a result of the upcycling process. X-ray diffraction (XRD) (Fig. 4a) indicates that Mg_2Si is the dominant precipitate phase in the recycled material. In the upcycled material, η'/$Mg(CuZn)_2$ is present in addition to Mg_2Si. High-angle annular dark field-scanning transmission electron microscopy (HAADF-STEM) reveals the presence of numerous Guinier-Preston (GP) zones along with several ordered precipitates within the Al matrix (Fig. 4b). A high-magnification bright field (BF) image, also shown in Fig. 4b, confirms that the structure of the ordered precipitates is consistent with that of the η' phase[18, 19]. Interestingly, we also found evidence that reaction occurs between pre-existing Mg_2Si particles and dissolved alloying elements Cu and Zn. As shown in Fig. 4c, new phases (rich in Cu and Zn) form next to Mg_2Si particles. High-resolution transmission electron microscopy reveals that the newly formed phases are amorphous Mg(ZnCu), with crystalline η' phase/$Mg(CuZn)_2$ within the amorphous phase. More detailed information is provided in **Fig. S3** (Supplementary Material Section 3) Three-dimensional atom maps of Al, Zn, Mg, and Cu distributions in the upcycled sample (Fig. 4d) reveal fluctuations in the Zn and Mg atom distributions within the Al matrix. The frequency distribution of the second nearest neighbor (2NN) distance (**Fig. S4a**) reveals the presence of clusters consisting of Zn, Mg, and Cu atoms. Figure 4e shows various crystallographic poles observed from the desorption map of the Atom Probe Tomography (APT) dataset. The stacking of $(11\bar{1})$ atomic planes are clearly resolved in the Al map along the [111] crystallographic pole (Fig. 4f). The Mg, Zn, and Cu map (Fig. 4g) shows spherical (green arrow) and elongated (red arrow) precipiates on the ($11\bar{1}$) planes, which correspond to Guinier-Preston I (GPI) and GPII zones [20–22], respectively. The number density of the GP zones is calculated to be ~ 1.6×10^{24} m^{-3} (**Fig. S4b**). These results provide strong evidence that solid-phase alloying is achieved during the upcycling process.

Typically, the development of GP zones within an Al matrix relies on two key factors: first, the matrix must be in a supersaturated solid solution state, usually achieved through a combination of solution heat treatment and rapid quenching. Second, there should be a low-temperature artificial aging [23] or room-temperature natural aging [24], during which GP zones nucleate and grow. However, subjecting the material to plastic deformation after attaining a supersaturated solid solution state can significantly expedite the aging process. This acceleration is attributed to dislocations generated during plastic deformation serving as nucleation sites for GP zone formation [25, 26]. Recent research has demonstrated that continuous plastic deformation can facilitate the direct formation of GP zones without the need for further aging steps. For instance, cyclic deformation of a supersaturated aluminum alloy at room temperature results in the dynamic precipitation of solute clusters (GP zones) by continuously introducing vacancies into the matrix [27]. Similar observations have been made in supersaturated magnesium alloys, where equal channel angular extrusion generates excess vacancies, leading to solute segregation and direct GP zone formation [28]. In the current study, the precursor materials are not in a supersaturated condition. Consequently, we hypothesize that two processes occur essentially simultaneously during the upcycling process: (1) dissolution of alloying additions into the matrix to

create a supersaturated solid solution, and (2) formation of GP zones due to the continuous generation of vacancies through severe plastic deformation.

The disparity in strength between recycled and upcycled materials (Fig. 2f) arises from the observed microstructural variations which can activate various strengthening mechanisms, such as grain boundary strengthening, solid solution strengthening, dislocation strengthening, and precipitate strengthening. Differences in grain size contribute to the strength increase, specifically with σ_{gb} (grain boundary strengthening) values of 43.2 MPa for upcycled materials and 13.1 MPa for recycled materials (refer to Supplementary Material Section 4 for detailed calculations). Alloying content variations also play a significant role in the strength difference, leveraging both solid solution strengthening and precipitate strengthening mechanisms. In particular, σ_{ss} (solid solution strengthening) values for upcycled and recycled materials are 46.8 MPa and 7.4 MPa, respectively (detailed calculations in Supplementary Material Section 5). The assessment of precipitate strengthening relies on the 3D atom probe analysis findings depicted in Fig. 4d. Notably, the presence of η' precipitates is considered insignificant for strength calculations. However, the presence of GP zones has a significant effect. The 3D atom probe analysis provides details on the average size and volume fraction of GP zones in the upcycled specimen, with strength contributions (σ_{Orowan}) from GP zones amounting to 115.9 MPa. Note that the strength attributed to GP zones (coherent to the Al matrix) is anticipated to result from a dislocation shearing mechanism (σ_{CS}) rather than an Orowan dislocation bypassing mechanism (σ_{Orowan}). However, the calculation revealing σ_{Orowan} to be smaller than σ_{CS} implies that Orowan dislocation bypassing is the operative mechanism for GP zones in this case. A comprehensive description of the calculation is provided in Section 6 of the Supplementary Material. It is crucial to note that the recycled specimen lacks GP zones, making the determined σ_{Orowan} from GP zones in the upcycled specimen an indicative measure for the precipitate strength contrast between the recycled and upcycled specimens. The variation in dislocation density does not significantly influence the strength difference, with (σ_d) (dislocation strengthening) values of 52.3 MPa for upcycled and 56.7 MPa for recycled specimens (refer to Supplementary Material Section 7 for detailed calculations). In total, theoretical calculations predict a yield strength improvement of 181 MPa in the upcycled aluminum, versus the recycled aluminum, in good agreement with the measured difference of 176 MPa.

In summary, a high-performance Al alloy is obtained by upcycling 6063 scrap with copper, zinc, and magnesium in a single-step, solid-phase alloying process. The yield and ultimate tensile strength of the upcycled material is increased by > 200% compared to the recycled material, due primarily to the formation of GP zones. These results demonstrate that low-strength and low-cost Al alloy scrap can be upcycled to high-strength and high-value Al alloy products by incorporating alloying elements via scalable solid-phase processing (friction extrusion), without the need to melt the precursor materials. Severe shear deformation imposed during friction extrusion refines the alloy additions and facilitates their uniform dispersion in the Al matrix, leading to the formation of fine GP zones and η'/$Mg(CuZn)_2$. Of larger significance, these results provide a first demonstration of a novel approach to alloy design and manufacturing that creates value from waste, reduces the energy footprint and environmental impact of

metals production, and offers a pathway to entirely new alloys and composites that cannot be produced by conventional melt-based proesses.

Methods

Base materials and tooling

- 6063 Al alloy scrap, Zn powders, Cu powders, and ZK60 Mg alloy ribbons were used as feedstock materials in this study. The chemical compositions of the 6063 Al alloy and ZK60 Mg alloy are provided in Table 1. A ZK60 Mg alloy was selected instead of pure Mg to avoid flammability issues. The chemical composition of the target 7075 Al alloy is also listed in Table 1.
- Friction extrusion tooling was made of H-13 tool steel. Spiral grooves were machined into the die face to facilitate material flow into the extrusion orifice, with a diameter of 5 mm. Die temperature was measured during processing using a type-K thermocouple (TC) spot-welded approximately 0.5 mm back from the die face.

Table 1
Nominal chemical composition of 6063 scrap, additional alloying powders and ribbons, mixed precursor, and standard 7075 [29].

Material	Chemical composition (wt. %)						
	Al	Mg	Si	Zn	Cu	Fe	Zr
6063 scraps	Bal.	0.45	0.4	0.02	0.02	0.2	-
Cu powders	-	-	-	-	100	-	-
Zn powders	-	-	-	100	-	-	-
ZK60 ribbons	-	Bal.	-	5–5.5	-	-	0.57
Mixed precursor	Bal.	2.5	0.4	5.6	1.6	0.2	0.01
Standard 7075 Al	Bal.	2.1–2.5	0–0.5	5.6–6.1	1.2–1.6	0–0.5	0

• Friction extrusion process

The manufacturing process for the recycled and upcycled rods is illustrated in Fig. 5. First, precursor scrap and alloying elements were weighed out according to the chemical compositions shown in **Table. 1**. Based on the amount of 6063 scrap and the additional additives, the final weight percentages of Mg, Cu, and Zn in the upcycled material were approximately 2.5%, 1.6%, and 5.6%, respectively. Second, the precursor materials were loaded into a plastic bottle, and the bottle was sealed and placed on a roller mixer for 1 hour. Third, the premixed precursor was loaded into a billet container and cold compacted with ~ 110 MPa using a hand press. Then, the liner with the pre-compacted precursor was loaded for friction extrusion into a ShAPE™ machine manufactured by Bond Technologies. Critical friction extrusion parameters, such as starting and steady-state spindle speed and plunge speed are listed in Table 2.

Table 2
Critical friction extrusion parameters for recycling and upcycle processes.

Process	Starting material	Spindle speed (RPM)	Plunge speed (mm/min)
Recycle	6063 Al alloy scrap	From 300 to 100	From 6 to 4 and 2
Upcycle	6063 Al alloy scraps + Zn powders + Cu powders + ZK60 Mg alloy ribbons	From 300 to 100	From 6 to 4 and 2

• Sample preparation

- Friction extrusion specimens were cut along the transverse cross-section and longitudinal cross-section using a diamond blade. Specimens for microstructural analysis were mounted in epoxy and polished to a final surface finish of 0.05 μm using colloidal silica.
- Three mini-tensile specimens were machined from the 5 mm diameter extruded rods for both the recycled and upcycled materials. The round bar specimens had a 38.1 mm total length and 15.88 mm gage length, following the ASTM-E8 standard.

• Microstructural characterization

- Optical microscopy was performed using an Olympus BX-51 fluorescence motorized microscope.
- Scanning electron microscopy (SEM) was performed using a Thermo Fisher Scientific Quanta 200 focused ion beam (FIB)-SEM outfitted with an Oxford Instruments X-ray energy dispersive spectroscopy (EDS) system for compositional analysis. Electron backscatter diffraction (EBSD) was done using a Thermo Fisher Scientific Apreo 2S SEM with an Oxford Instruments EBSD detector operating at 20 kV and step size of 0.2 μm. The EBSD results were analyzed using ZtecCrystal EBSD processing software.
- Transmission electron microscopy (TEM) specimens were prepared by following the routine lift-out and thinning procedure of the FIB technique on a Thermo Fisher Scientific Quanta 200 FIB-SEM or a Thermo Fisher Scientific Helios 5 Hydra Dual Beam plasma focused ion beam milling scanning electron microscopy (PFIB-SEM).
- TEM/scanning TEM (STEM) observations were performed on an FEI (now Thermo Fisher Scientific) Titan 80–300 Environmental Cs-corrected TEM equipped with an EDS system. High-angle annular dark field (HAADF) and bright field (BF)-scanning transmission electron microscopy (STEM) images were captured on a JEOL GrandARM-300F operating at 300 kV with a convergence semi-angle of 29.7 mrad. The collection angles for HAADF-STEM were between 75 and 515 mrad.
- X-ray diffraction analysis was performed using a Rigaku D/Max Rapid II microdiffraction system. Diffraction data recorded on a two-dimensional image plate were integrated for diffraction angles between 20° and 150° using the manufacturer's software (2D Data Processing Software v.1.0, Rigaku, 2007).

- 3D atom probe (3DAP) analysis was performed using a local electrode atom probe (CAMECA LEAP 6000 XR) in voltage pulse mode with a pulse fraction of 20% at a temperature of 40 K. Sharp needle-like specimens for the 3DAP analysis were prepared by the FIB lift-out and annular milling techniques using an FEI Helios 5 Hydra UX. The statistics and chemistry of precipitates in the selected volume without the Al poles were analyzed using a maximum separation algorithm in the AP Suite™ 6.3 software. The parameters of separation distances (d_{max} = 0.58), minimum number of solutes (N_{min} = 12), envelop distances (L = 0.58), and erosion distances ($d_{erosion}$ = L) were selected based on the nearest neighbor approach described elsewhere [30].

• Mechanical property characterization

- Hardness values for the recycled and upcycled materials were measured on the cross-section using a Vickers microhardness tester at 200 g load, with a dwell time of 12 s.
- Tensile tests were carried out on an MTS mechanical testing machine using a constant rate of 0.08 mm/min along with digital image correlation analysis measuring deformation strain.

Declarations

Declaration of Competing Interest

The authors declare that they have no known competing financial interests or personal relationships that could have appeared to influence the work reported in this paper.

Acknowledgments

Pacific Northwest National Laboratory (PNNL) is a multiprogram national laboratory operated by Battelle for the DOE under Contract DEAC05-76RL01830. Current work was supported by the Laboratory Directed Research and Development (LDRD) program at PNNL as part of the Solid Phase Processing Science Initiative (SPPSI). The authors are grateful for the efforts of Anthony Guzman for the preparation of specimens for microstructural characterization. This work was performed, in part, at the William R. Wiley Environmental Molecular Sciences Laboratory, a national scientific user facility sponsored by U.S. Department of Energy, Biological and Environmental Research program located at PNNL.

Funding

This work was supported by the Laboratory Directed Research and Development program at PNNL as part of the SPPSI.

References

1. Totten, G.E. and D.S. MacKenzie, *Handbook of aluminum: vol. 1: physical metallurgy and processes*. Vol. 1. 2003: CRC press.

2. Ungureanu, C., S. Das, and I. Jawahir, *Life-cycle cost analysis: aluminum versus steel in passenger cars.* TMS (the minerals, metals & materials society), 2007. **1**: p. 11-24.
3. Raabe, D., et al., *Making sustainable aluminum by recycling scrap: The science of "dirty" alloys.* Progress in materials science, 2022. **128**: p. 100947.
4. Raabe, D., *The materials science behind sustainable metals and alloys.* Chemical Reviews, 2023. **123**(5): p. 2436-2608.
5. Das, S.K., et al., *Aluminum recycling—An integrated, industrywide approach.* JOM, 2010. **62**: p. 23-26.
6. Green, J.A., *Aluminum recycling and processing for energy conservation and sustainability*. 2007: ASM International.
7. Kelly, S. and D. Apelian, *Automotive aluminum recycling at end of life: a grave-to-gate analysis.* Center for Resource Recovery and Recycling (CR3), Metal Processing Institute, Worcester Polytechnic Institute, 2016. http://www. drivealuminum. org/wp-content/uploads/2016/06/Final-Report-Automotive-Aluminum-Recycling-at-End-of-Life-A-Grave-to-Gate-Analysis. pdf, Accessed July 2018, 2018.
8. MINODA, T., H. HAYAKAWA, and H. YOSHIDA, *Effect of iron content on the surface quality of 6063 aluminum alloy extrusion.* Keikinzoku, 2000. **50**(10): p. 491-494.
9. Gnatko, M., et al., *Purification of aluminium cast alloy melts through precipitation of Fe-containing intermetallic compounds.* Metals, 2018. **8**(10): p. 796.
10. Bushi, L., T. Skszek, and T. Reaburn, *New ultralight automotive door life cycle assessment.* The International Journal of Life Cycle Assessment, 2019. **24**: p. 310-323.
11. Akar, S., C. Kinchin, and P. Kurup, *Techno-Economic Analysis for Shear Assisted Processing and Extrusion (ShAPE) of High Strength Aluminum Alloys*. 2022, National Renewable Energy Lab.(NREL), Golden, CO (United States).
12. Taysom, B.S., et al., *Fabrication of aluminum alloy 6063 tubing from secondary scrap with shear assisted processing and extrusion*, in *Light Metals 2022*. 2022, Springer. p. 294-300.
13. Li, X., et al., *Copper carbon composite wire with a uniform carbon dispersion made by friction extrusion.* Journal of Manufacturing Processes, 2021. **65**: p. 397-406.
14. Li, X., D. Baffari, and A. Reynolds, *Friction stir consolidation of aluminum machining chips.* The International Journal of Advanced Manufacturing Technology, 2018. **94**: p. 2031-2042.
15. Wang, T., et al., *Extrusion of unhomogenized castings of 7075 aluminum via ShAPE.* Materials & Design, 2022. **213**: p. 110374.
16. Li, L., et al., *Analysis of contact conditions and microstructure evolution in shear assisted processing and extrusion using smoothed particle hydrodynamics method.* Materials & Design, 2022. **221**: p. 111010.
17. Li, X., et al., *Strain and strain rate in friction extrusion.* Journal of Materials Research and Technology, 2022. **20**: p. 882-893.

18. Li, X., et al., *HREM study and structure modeling of the η′ phase, the hardening precipitates in commercial Al–Zn–Mg alloys.* Acta materialia, 1999. **47**(9): p. 2651-2659.
19. Zhang, X., et al., *Atomic-scale study on the precipitation behavior of an Al–Zn–Mg–Cu alloy during isochronal aging.* Journal of Materials Science & Technology, 2022. **108**: p. 281-292.
20. Sha, G. and A. Cerezo, *Early-stage precipitation in Al–Zn–Mg–Cu alloy (7050).* Acta materialia, 2004. **52**(15): p. 4503-4516.
21. Liu, J., et al., *Formation of solute nanostructures in an Al–Zn–Mg alloy during long-term natural aging.* Journal of Alloys and Compounds, 2020. **821**: p. 153572.
22. Lee, S.-H., et al., *Precipitation strengthening in naturally aged Al–Zn–Mg–Cu alloy.* Materials Science and Engineering: A, 2021. **803**: p. 140719.
23. Hu, T., et al., *Precipitation phenomena in an ultrafine-grained Al alloy.* Acta Materialia, 2013. **61**(6): p. 2163-2178.
24. Zheng, G.W., et al., *Natural aging behaviors and mechanisms of 7050 and 5A90 Al alloys: A comparative study.* Materials Science and Engineering: A, 2018. **718**: p. 157-164.
25. Shanmugasundaram, T., B.S. Murty, and V. Subramanya Sarma, *Development of ultrafine grained high strength Al–Cu alloy by cryorolling.* Scripta Materialia, 2006. **54**(12): p. 2013-2017.
26. Zhao, Y.H., et al., *Microstructures and mechanical properties of ultrafine grained 7075 Al alloy processed by ECAP and their evolutions during annealing.* Acta Materialia, 2004. **52**(15): p. 4589-4599.
27. Sun, W., et al., *Precipitation strengthening of aluminum alloys by room-temperature cyclic plasticity.* Science, 2019. **363**(6430): p. 972-975.
28. Sasaki, T.T., et al., *Deformation induced solute segregation and G.P. zone formation in Mg-Al and Mg-Zn binary alloys.* Scripta Materialia, 2022. **220**: p. 114924.
29. Committee, A.H., *Properties of wrought aluminum and aluminum alloys.* ASM handbook, 1990. **2**: p. 62-122.
30. Jägle, E.A., P.-P. Choi, and D. Raabe, *The maximum separation cluster analysis algorithm for atom-probe tomography: Parameter determination and accuracy.* Microscopy and Microanalysis, 2014. **20**(6): p. 1662-1671.

Figures

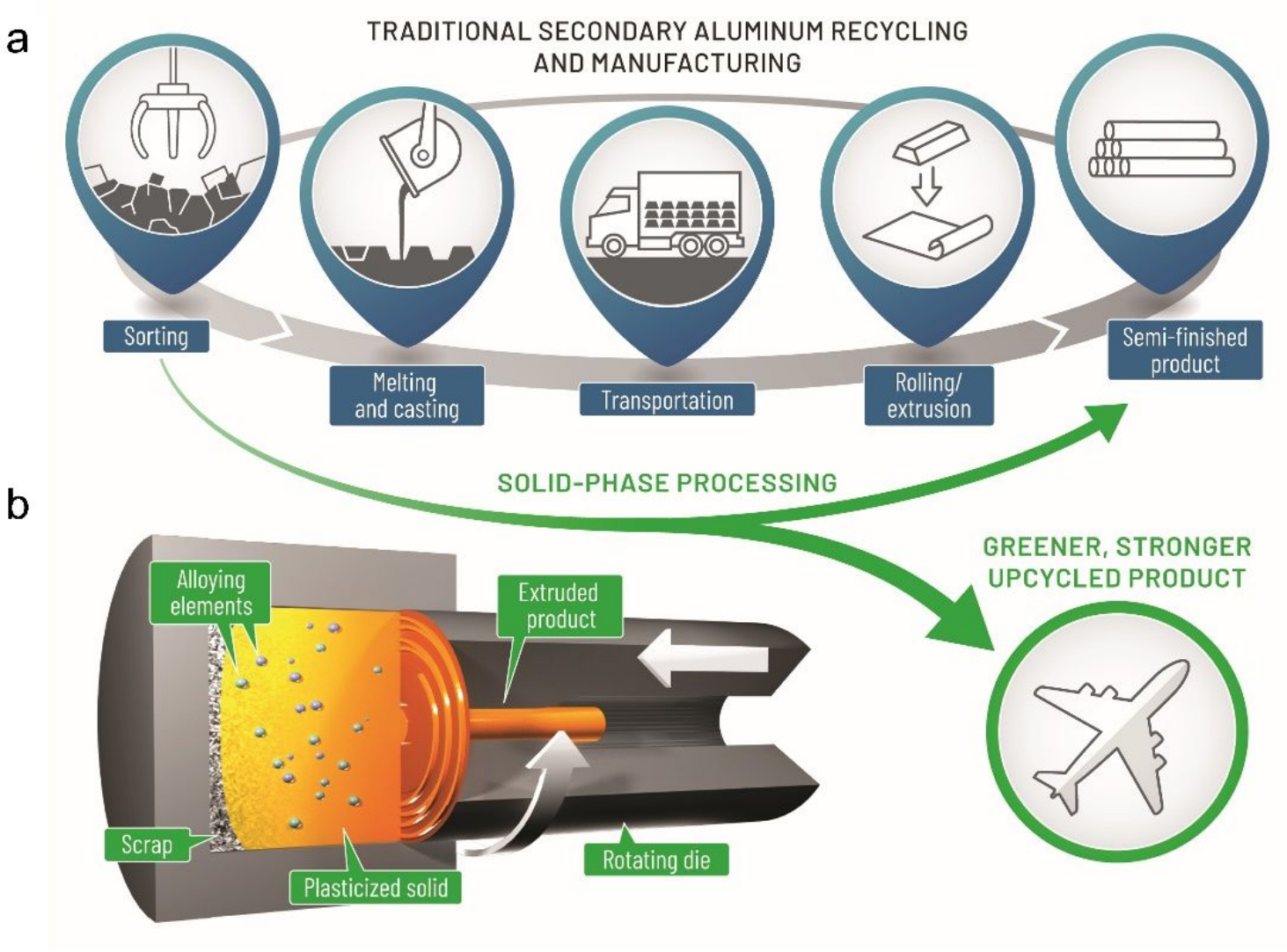

Figure 1

Aluminum life cycle and the upcycle workflow.

a. Traditional secondary Al recycling and manufacturing route: sorting, melting and casting, transportation, rolling/extrusion, and semi-finished products (rod, bar, and sheet). **b**. Solid-phase processing directly recycles or upcycles scrap into extrudate via friction extrusion and reduces energy consumption by avoiding energy-intensive steps.

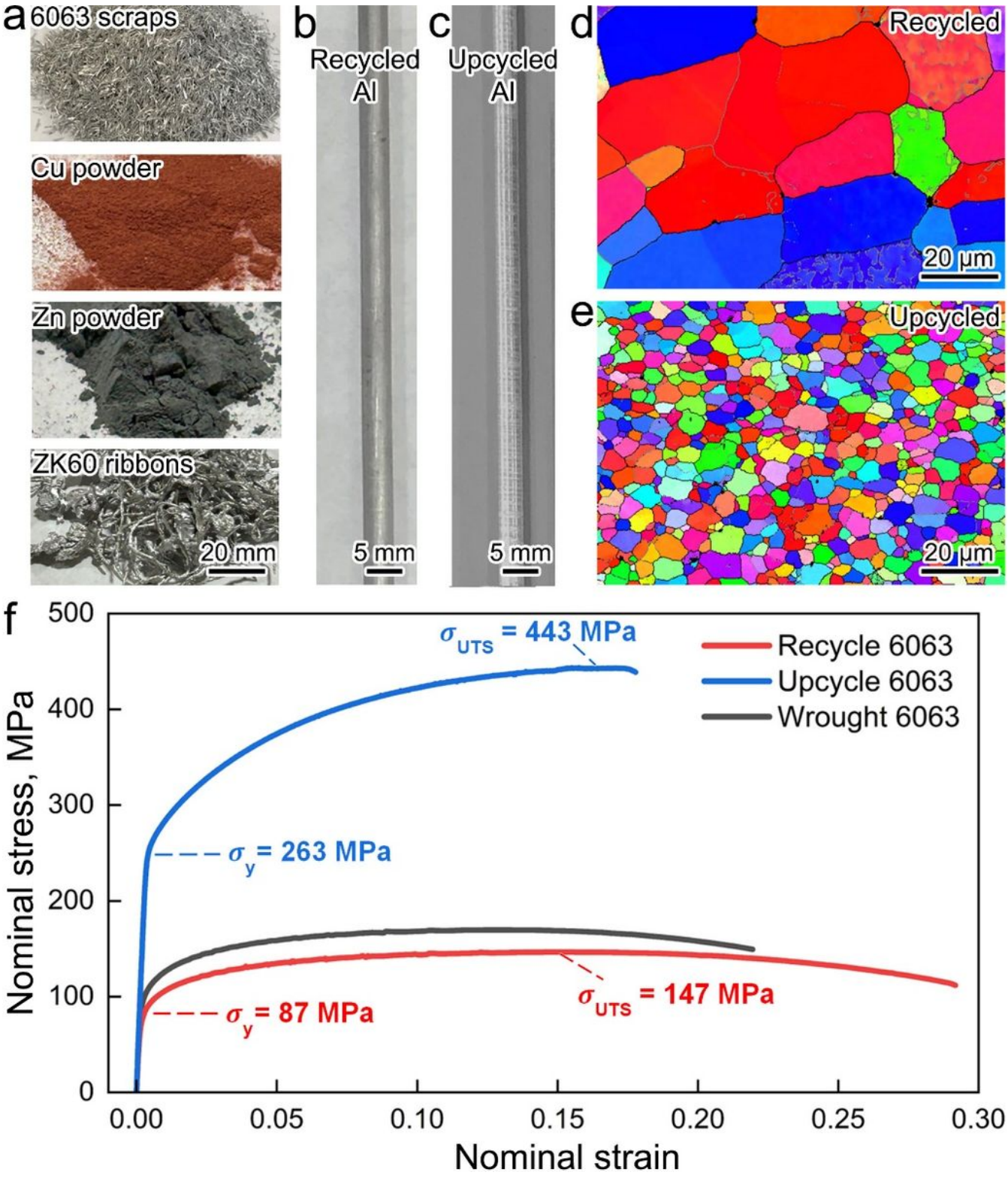

Figure 2

Friction-extruded rods and their respective mechanical properties

a. Al scrap and alloying additions used in friction extrusion recycling and upcycling, from top to bottom: 6063 Al scrap, copper powder, zinc powder, and ZK60 magnesium alloy ribbons. **b**. Recycled Al rod made only from cold compacted 6063 Al scrap. **c**. Upcycled Al rod made from a mixture of 6063 Al scrap with

alloying additions. **d**. EBSD-IPF showing the grain morphology of a recycled Al rod. **e**. EBSD-IPF showing the grain morphology of the upcycled Al rod. **f**. Stress-strain curves of friction-extruded samples: recycled Al rod and upcycled Al rod, compared with a commercial wrought 6063 Al alloy.

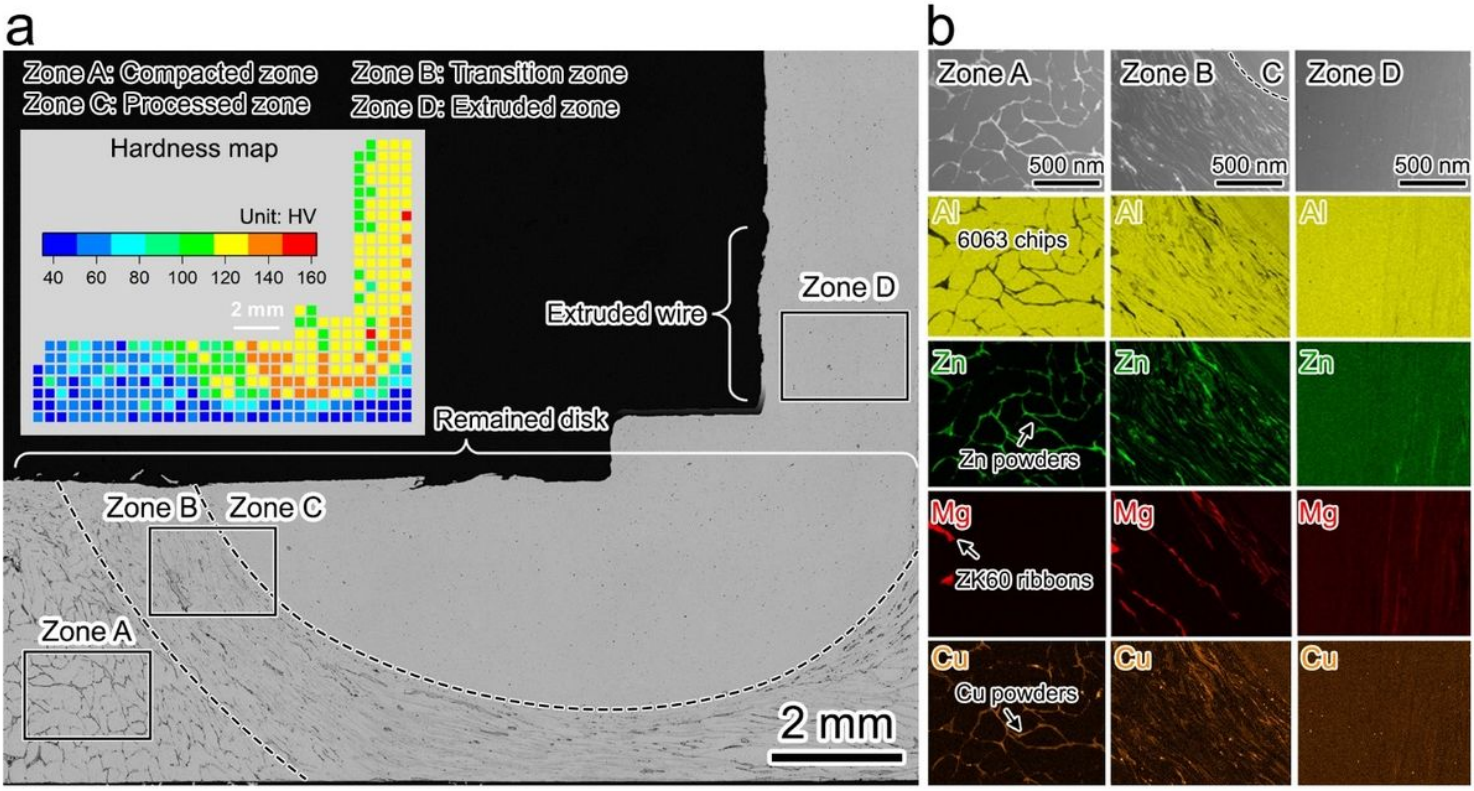

Figure 3

Microstructural evolution during solid-phase alloying

a. Optical image displaying four distinct regions from bottom to top—Zone A: compacted scrap, powders, and ribbons; Zone B: deformed materials transition from compacted microstructure to processed microstructure; Zone C: mixed and alloyed microstructure; Zone D: extruded microstructure. Note the hardness map inset in **Fig. 3a**, covering the span from Zone A to Zone D. **b**. SEM and EDS mapping of Al, Zn, Mg, and Cu (from top to bottom) at Zone A, Zone B, and Zone D (from left to right).

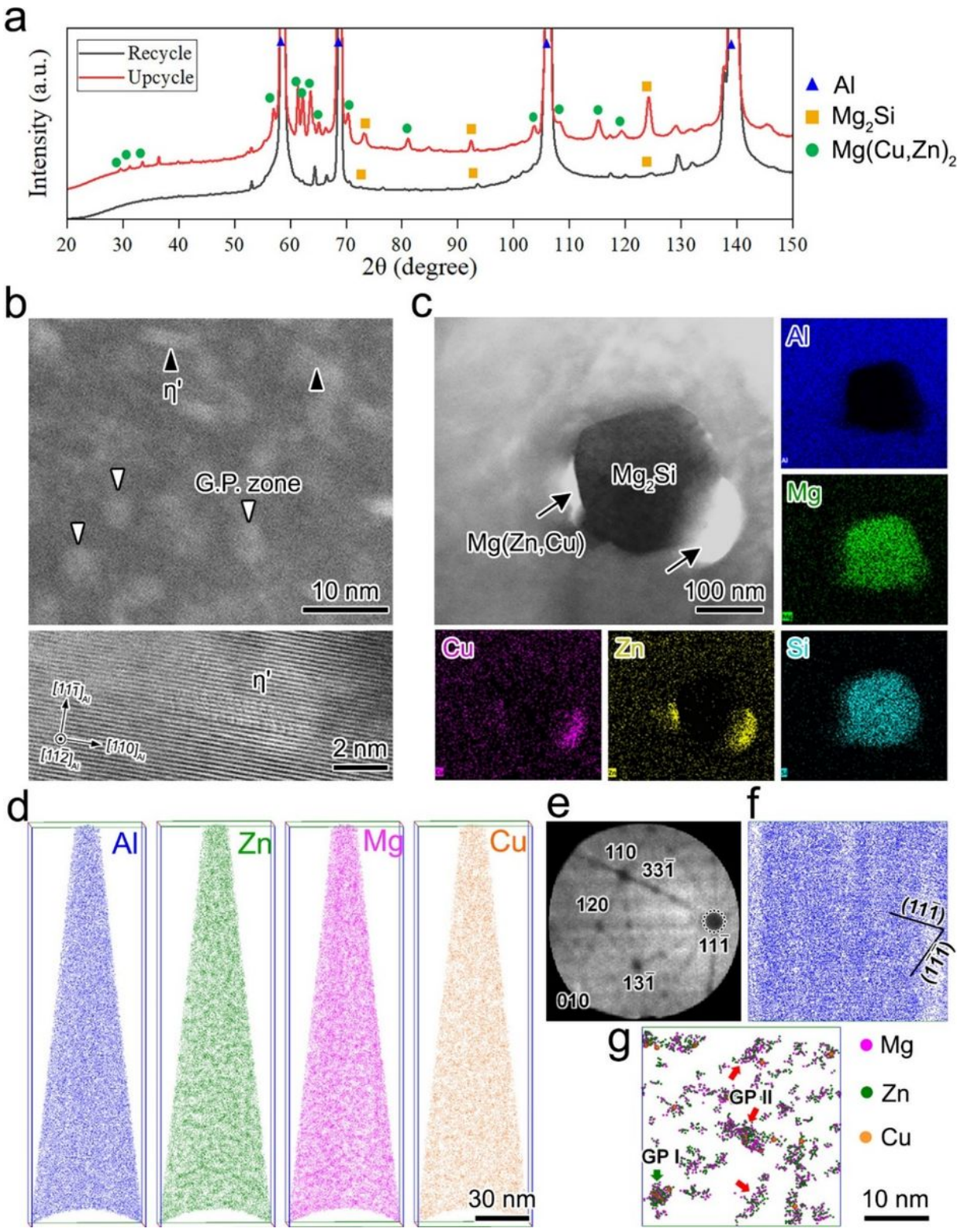

Figure 4

Phase identification and microstructure of the recycled and upcycled Al via solid-phase process

a. XRD analysis on the recycled and upcycled Al indicated that new $Mg(CuZn)_2$ phases were formed in the upcycling process. **b**. HAADF and BF images on the upcycled specimen reveal the existence of GP zone and η' phase nanoclusters. **c**. Transmission electron microscopy and EDS analysis on pre-existed

Mg_2Si particles reacting with newly dissolved Zn and Cu. They show potential reaction products next to pre-existing Mg_2Si particles. **d**. 3D atom maps of Al, Zn, Mg, and Cu in the upcycled specimen. **e**. The desorption map of the entire atom probe tomography dataset with indexed crystallographic poles. **f** and **g**. Sliced atom maps of Al, Zn, Mg, and Cu along the [$11\bar{1}$] pole of a selected volume with dimensions of $30 \times 30 \times 30\ nm^3$.

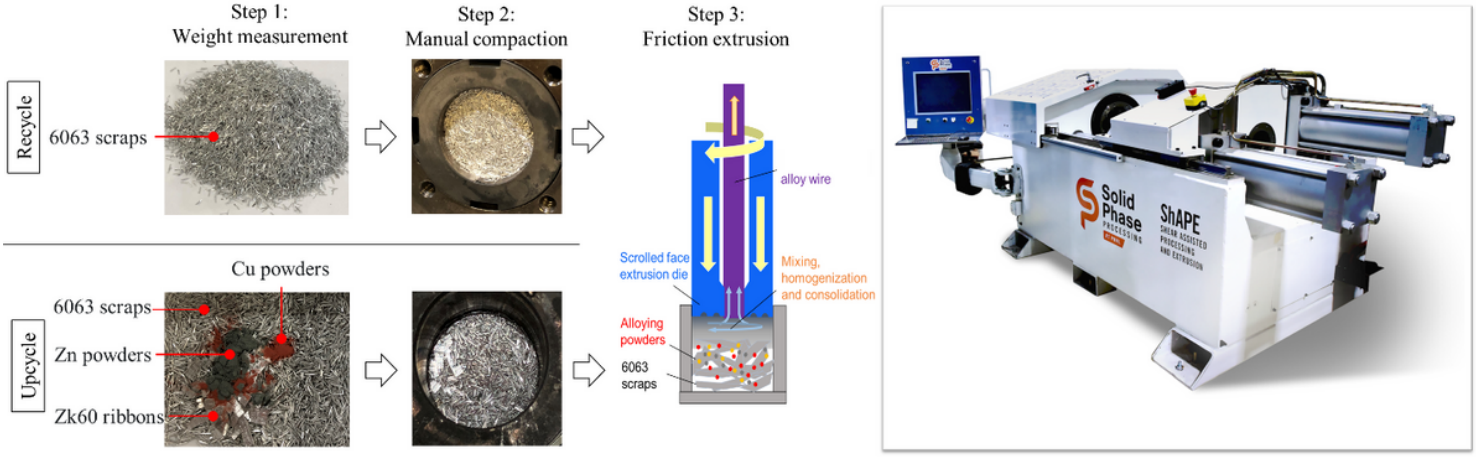

Figure 5

Experiment procedures for both recycling and upcycling from weight measurement of chips and powders to compaction and friction extrusion.

Supplementary Files

This is a list of supplementary files associated with this preprint. Click to download.

- Supplementary.docx